

MUSES: multi-sensor soil electromagnetic sounding

G. Vannaroni^{a,*}, E. Pettinelli^b, C. Ottonello^c, A. Cereti^{a,b}, G. Della Monica^b, D. Del Vento^{a,b},
A.M. Di Lellis^d, R. Di Maio^e, R. Filippini^c, A. Galli^f, A. Menghini^g, R. Orosei^h, S. Orsini^a,
S. Pagnan^c, F. Paolucci^b, A.R. Pisani^b, G. Schettiniⁱ, M. Storini^a, G. Tacconi^c

^a*Istituto di Fisica dello Spazio Interplanetario, CNR, via del Fosso del Cavaliere 100, Rome 00133, Italy*

^b*Dipartimento di Fisica "E. Amaldi", Università Roma Tre, Rome, Italy*

^c*Istituto di Studi sui Sistemi Intelligenti per l'Automazione, CNR, Genoa, Italy*

^d*AMD L, Rome, Italy*

^e*Dipartimento Scienze Fisiche, Università di Napoli "Federico II", Naples, Italy*

^f*Dipartimento di Ingegneria Elettronica, Università di Roma "La Sapienza", Rome, Italy*

^g*S. Te. G. A. Studio di Tecnologie per la Geologia e per l'Ambiente, Viterbo, Italy*

^h*Istituto di Astrofisica Spaziale e Fisica Cosmica, CNR, Rome, Italy*

ⁱ*Dipartimento di Elettronica Applicata, Università Roma Tre, Rome, Italy*

Received 14 January 2003; received in revised form 12 June 2003; accepted 29 August 2003

Abstract

The authors describe the performance of a multi-sensor package designed to measure the electromagnetic properties of the subsurface during future landing missions to Mars. The package consists of a soil dielectric spectroscopy probe (SDSP), a ground penetrating radar (GPR) and a time domain electromagnetic measurement (TDEM) system that, using different methods, estimate the electromagnetic properties of the shallow subsurface at different depths (0–100 m). A data fusion approach is considered to improve the reliability and accuracy of the measurements.

© 2003 Elsevier Ltd. All rights reserved.

Keywords: Electromagnetic sounding; Subsurface radar; Dielectric spectroscopy; Complex permittivity

1. Introduction

The reconstruction of the Mars shallow subsurface structure and the detection of water can be performed with the aid of different geophysical techniques. The variation in mineral composition, porosity, water content, and salinity correspond to variation in the physical properties of the soil or rock. Because geophysical methods locate boundaries across which there is a marked contrast in physical properties, they can supply useful information about the geometry and nature of the subsurface structure.

Among the large variety of well-established geophysical methods used on the Earth for subsurface exploration, electromagnetic (e.m.) surveys are, by far, the most suitable for a planetary mission, because they are relatively simple and appropriate to be hosted on a moving vehicle. These techniques rely on the e.m. parameters of the subsoil

and are sensitive to the contrast of conductivity, permittivity and magnetic permeability of the subsurface lithology. The e.m. techniques can be applied in both time and frequency domains and can investigate the subsurface at various ranges of depths.

Usually, when a geophysical survey is required on the Earth just one technique (the most suitable to solve the specific problem) is used. This is because here additional information is easily accessible through outcrop examination or borehole data. It is important to notice, however, that no geophysical method by itself provides a unique solution to a particular geological situation. It is, therefore, of paramount importance that geophysical data are interpreted within a physically constrained or geological framework (Reynolds, 1998). In the case of Mars exploration, very few geological and petrologic data are available, and constraints that can be imposed to a subsurface model are minimal. To overcome this problem, the authors have proposed the use of a multi-sensor tool which can operate in both frequency and time domains, investigating different depths with differ-

* Corresponding author. Tel.: +39-06-49934356; fax: +39-06-49934383.

E-mail address: giuliano.vannaroni@ifsi.rm.cnr.it (G. Vannaroni).

ent resolutions. Multi-sensor soil electromagnetic sounding (MUSES) is an integrated instrument package, which consists of three sensors: the soil dielectric spectroscopy probe (SDSP), the ground penetrating radar (GPR), and the time domain electromagnetic measurement (TDEM) system.

The SDSP operates between 100 Hz and 1 MHz, measures the complex permittivity down to a depth which depends on the geometrical dimensions of the probe. It is particularly appropriate to identify elements characterized by high polarizability, which indicate the presence in the soil of water both in solid or liquid form. The GPR operates in the time domain, using antennas with a frequency range 200 MHz–1 GHz, and detects the geometry of the subsurface structures up to a depth of about 10 m. The TDEM determines the vertical profile of the subsoil conductivity in a large range of depths, extending from about 3 down to 100 m.

The use of different techniques in the same site will provide various advantages thanks to the competitive, cooperative and complementary features of the various sensors. In fact:

(i) If the subsurface is mainly resistive, i.e. low concentration of conductive minerals and low water content (liquid), the GPR signals can penetrate in depth. The GPR technique is, therefore, capable to produce a detailed (high resolution) imaging of the subsoil in terms of intrinsic impedance contrast, which depends on conductivity, permittivity and permeability of the material.

(ii) If the subsurface is mainly conductive, i.e. there is high concentration of conductive minerals and/or high liquid water content, the TDEM, being particularly responsive to a conducting medium, provides an accurate vertical profile of the subsoil conductivity.

(iii) If the first meter of the Mars subsurface contains water ice or liquid water, it can be detected from measurements of the permittivity by the SDSP; in particular, the water ice can be detected from its relaxation, which exhibits marked signatures of the complex permittivity at frequencies of the order of hundreds of Hz.

(iv) The complex permittivity obtained with SDSP can be used to determine the e.m. wave propagation velocity and improve the accuracy of the GPR data inversion.

(v) The fusion of the data collected by the three sensors yields better physical constraints on the geophysical model of the subsurface.

The paper is organized as follows. Section 2 describes a model of the Martian soil at shallow depths (derived from a preliminary analysis of the Odyssey satellite data), which is useful to establish the requirements of the various sensors in terms of operating range and performance. Section 3 illustrates the working principles of the SDSP, GPR and TDEM, and gives some simulation results related to exploration depth, accuracy, resolution and sensitivity. In Section 4, we discuss a data fusion approach capable of improving the overall accuracy of the observations, and present our concluding remarks.

2. A Martian shallow subsurface model

To accurately interpret the response of surface-penetrating e.m. sensors, a geophysical model of the subsurface composition and stratigraphy must be first analyzed, to evaluate the e.m. parameters of the ground at various depths. This approach helps to identify the properties that can be investigated by each sensor, and to define the baseline performance and limitations of MUSES.

Stratigraphy provides the variation of the rocks and soils features vs. depth. From the MUSES perspective, stratigraphy does not refer to the physical properties of the rocks and soils but to the distribution of their e.m. properties: conductivity, permittivity and permeability. The upper surface of Mars is largely a result of resurfacing by volcanic, fluvial, aeolian, periglacial, and impact processes. It is estimated that a layer of displaced materials may cover the planet with a thickness up to 2 km. This soil could contain a significant amount of water ice near the surface and liquid water at greater depths. On a smaller scale, it is likely that this ejecta (resurfaced) layer is discontinuously interbedded with volcanic flows, weathering products, and sedimentary deposits, all overlying a heavily fractured basement.

Measurements from the gamma-ray spectrometer (GRS) experiment onboard the Mars Odyssey spacecraft (Boynton et al., 2002; Feldman et al., 2002; Mitrofanov et al., 2002) appear to confirm the existence of possibly large quantities of shallow subsurface water ice in some areas of the planet. GRS measures the neutron flux emitted from Mars and the spectra of gamma-ray emissions induced by neutron capture reactions. The experiment maps, for the first time, the global distribution of near-surface hydrogen on the planet. The abundance of hydrogen varies widely. The highest concentrations occur poleward from about 60°N and 60°S and might reveal the presence of subsurface water ice in regions where ground ice has been predicted to be stable. A first modeling of the experimental results indicates that the best fits for the enhanced hydrogen regions are consistent with a surface made of a “thin and dry” upper layer (i.e. few tens of centimeters, 1–2 (wt% H₂O) over a “thick and ice-rich” lower stratum (several hundred centimetres, 20–35 wt% H₂O). Information on the thickness of the ice-rich lower layer is limited by the sensing depth of the neutron instruments (\cong 1 m), and it is not possible to determine the total quantity of subsurface ice present. However, if the modeling is correct, then the inferred ice concentration implies an extremely porous, nearly ice-filled regolith at high latitudes.

3. Description of the MUSES sensors

3.1. SDSP working principle

The SDSP determines the complex permittivity of the shallow subsoil from measurements of the mutual

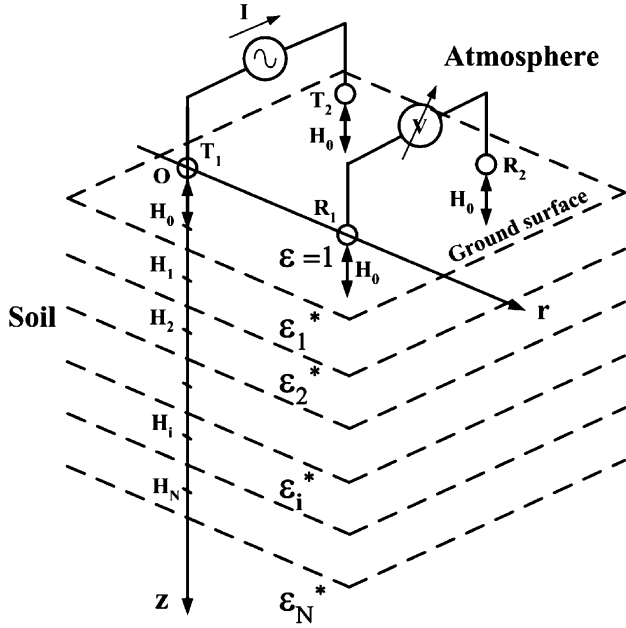


Fig. 1. SDSP electrode square array configuration above a layered soil.

impedance of a four-electrode system electrically coupled with the ground. The mutual impedance is defined as the ratio of the voltage measured across a pair of receiving electrodes to the current transmitted by a second pair of electrodes (see Fig. 1). The measurements are performed in AC regime and the electrodes do not require low impedance DC contacts with the soil. In fact, the terminals are capacitively coupled to the terrain and do not require any galvanic contact. This feature is particularly important in that the sensors are envisaged to be installed on a moving vehicle for planetary exploration. The use of a capacitively coupled system for the electrical survey of soils has been first studied and proposed by Grard (1990a, b) and Grard and Tabbagh (1991). The band of frequency is limited to the range 100 Hz–1 MHz. The lower bound is required to maintain the current injected through the soil at measurable levels, on the other hand, the upper frequency limits the range over which the quasi-static approximation can be applied in the data inversion analysis (Tabbagh et al., 1993). The SDSP provides information about the water content in the soil both in liquid and solid phases. In particular, the moisture in the ground can be estimated as the dielectric constant of water ($\cong 78$) is much higher than that of a dry soil, which is in the range 2–15. On the other hand, the identification of water ice is obtained from the response of the sensor as a function of frequency. In fact, the relaxation process of ice produces marked variations of the complex permittivity at frequencies from several hundreds of Hz to a few kHz, for soil temperatures between -50°C and 0°C , respectively (Zhadanov and Keller, 1998; Von Hippel, 1988 and references therein).

The general equation, which is at the basis of the SDSP working principle, is Ohm's law generalized to dielectric materials with losses

$$J_{\text{tot}} = j\omega\epsilon_0\epsilon^*E, \quad (1)$$

where the relative complex permittivity is defined as

$$\epsilon^* = \epsilon' - j\left(\frac{\sigma}{\omega\epsilon_0} + \epsilon''_d\right). \quad (2)$$

The real part of ϵ^* is the relative dielectric constant (associated with the polarizability of the material); the imaginary part represents the effects of the DC conductivity (σ) and the dissipation associated to the polarization process (Chelidze and Gueguen, 1999). Usually, at operating frequencies < 1 MHz, the term ϵ''_d is negligible with respect to $\sigma/\omega\epsilon_0$, and the imaginary part of Eq. (2) reduces to $\epsilon'' = \sigma/\omega\epsilon_0$.

The potential difference between the receiver electrodes R_1 and R_2 (Fig. 1) can be evaluated from the continuity equation of the electric current and Laplace's equation solution (along with the boundary conditions) (Grant and West, 1965).

The interpretation and inversion of the measurements require some assumptions on the soil stratigraphy. We have considered two simplified models based on homogeneous and layered soil, respectively.

For the homogeneous soil, it can be shown that the real and imaginary components of the mutual impedance $Z^*(\omega) = R(\omega) + j\omega X(\omega)$ are (Vannaroni and Del Vento, 2003)

$$R = X_0 K \frac{2\epsilon''}{(\epsilon' + 1)^2 + \epsilon''^2},$$

$$X = -X_0 \left(1 - K \frac{\epsilon'^2 + \epsilon''^2 - 1}{(\epsilon' + 1)^2 + \epsilon''^2}\right), \quad (3)$$

where K and X_0 are quantities related to the geometrical dimensions of the array.

Assuming that the terminals graze the soil (i.e. $H_0 = 0$, see Fig. 1) we obtain, for a square array of electrodes with side d : $K = 1$ and $X_0 = (2 - \sqrt{2})/(4\pi\epsilon_0\omega d)$. Eqs. (3) can be easily inverted to obtain, from a given measured impedance, the real and imaginary parts of the complex permittivity of the soil (i.e. ϵ' and ϵ'').

On the other hand, for the multilayered ground the response of an electrostatic quadrupole can be calculated generalizing the treatment performed by Fechant et al. (1999) for a three layers, 1-D modeled medium. In such a case, the mutual impedance can be expressed by a functional relation of the type

$$Z_k^* = f_k(H_0, H_1, \dots, H_i, \dots, H_N, \epsilon_0, \epsilon_1^*, \dots, \epsilon_i^*, \dots, \epsilon_N^*), \quad (4)$$

where f_k is also function of the array geometry. The Z_k^* expressions contain integrals involving Bessel functions, as usually found in Geophysical problems characterized by cylindrical symmetry (Grant and West, 1965). The inversion of Eq. (4) requires a more complex treatment than that

needed for a homogeneous terrain, and is further complicated by the large number of unknowns (i.e. the complex permittivity and thickness of the various layers) and by the integrals that can be calculated only through numerical methods. However, if the measurements are repeatedly performed on the same site with different quadrupole geometries, we obtain several relations (each of the form of Eq. (4)) that can be solved to determine the permittivity and thickness of the various layers. This approach requires the arrangement of a multi-quadrupole system onboard the rover. The various arrangements should exhibit diverse geometries (i.e. different electrode array extensions) to achieve an independent set of equations.

In both cases (homogeneous and layered soil), the measurements performed with a quadrupole contain significant information down to a depth of the order of the separating distances between the electrodes ($\cong d$). Although several simulations have been carried out to study the inversion of the impedances measured by a multi-quadrupole probe on both homogeneous and stratified terrains, in this paper, for sake of brevity, only the performance achievable for homogeneous soils are reported.

3.2. SDSP accuracy on a homogeneous soil

The errors affecting the SDSP measures may be originated by the uncertainties associated to the mutual impedance measurements, by the discrepancies between the modeled and actual soil stratigraphy, and by the inaccuracy relevant to the electrode array deployment above the soil surface. Here we will discuss only the first type of error, assuming a homogeneous ground and perfectly known geometric configuration of the electrode array (square geometry with a side $d = 1$ m), which, in addition, grazes the soil (i.e. $H_0 = 0$).

The errors on the impedance rely mainly on the uncertainties associated to the electronic subsystems that perform the amplitude and phase measurements of the quadrupole voltages and currents. In this paper, we have supposed that the uncertainties are typical of commercial laboratory impedance analyzers, and we have considered errors on amplitude and phase $\Delta|Z|/|Z| \cong 0.2\%$ and $\Delta\varphi \cong 0.2^\circ = 3.5 \times 10^{-3}$ rad, respectively, where $|Z| = \sqrt{R^2 + X^2}$ and $\varphi = \text{tg}^{-1}(X/R)$.

The accuracies on ε' and ε'' have been estimated from Eqs. (3) where $\varepsilon'' = \sigma/\omega\varepsilon_0$. We have calculated the errors for soil conditions that could be of realistic interest for Mars exploration ($10^{-7} < \sigma < 10^{-2}$ S/m, and $1 < \varepsilon' < 80$).

The error analysis is summarized in Figs. 2 and 3, as a function of frequency and conductivity. It has been verified that the errors are mainly dependent on the operating frequency and soil conductivity, but only weakly affected by ε' (Vannaroni and Del Vento, 2003). Figs. 2 and 3 refer to the case $\varepsilon' = 3$ (typical value for a dry soil); however, the errors calculated with a fixed dielectric constant can be approximately extrapolated to higher values (as those expected

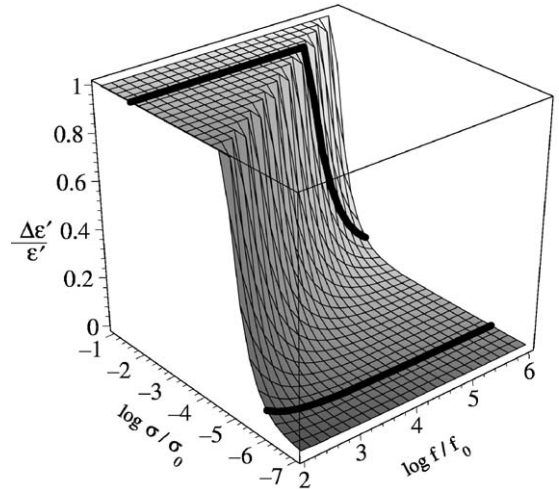


Fig. 2. Relative errors $\Delta\varepsilon'/\varepsilon'$ as a function of frequency and conductivity for $\varepsilon' = 3$ (the vertical scale is limited to 1 (i.e. error = 100%)). The two solid lines mark two different soil conductivities 10^{-6} and 10^{-2} S m $^{-1}$ (the logarithmic scales refer to $f_0 = 1$ Hz and $\sigma_0 = 1$ S m $^{-1}$).

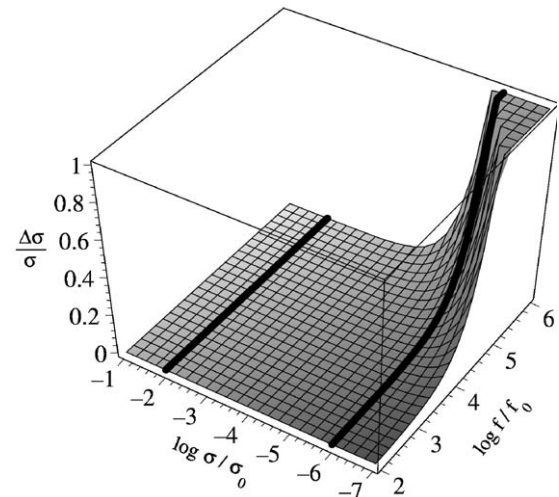


Fig. 3. Relative errors $\Delta\sigma/\sigma$ as a function of frequency and conductivity for $\varepsilon' = 3$ (the vertical scale is limited to 1 (i.e. error = 100%)). The two solid lines mark two different soil conductivities 10^{-6} and 10^{-2} S m $^{-1}$ (the logarithmic scales refer to $f_0 = 1$ Hz and $\sigma_0 = 1$ S m $^{-1}$).

for soils containing some moisture or magnetite (Pettinelli et al., 2003)). The errors on ε' and σ exhibit an opposite trend vs. frequency and soil conductivity. Indeed, while $\Delta\varepsilon'/\varepsilon'$ increases at low frequency and high conductivity, $\Delta\sigma/\sigma$ enhances at high frequency and low conductivity. Anyhow there is a relatively broad region of soil conductivity where the errors on both ε' and σ are relatively low and widely acceptable.

3.3. GPR working principle

GPR technique is a geophysical method, which uses radio waves, typically in the frequency range 10–3000 MHz,

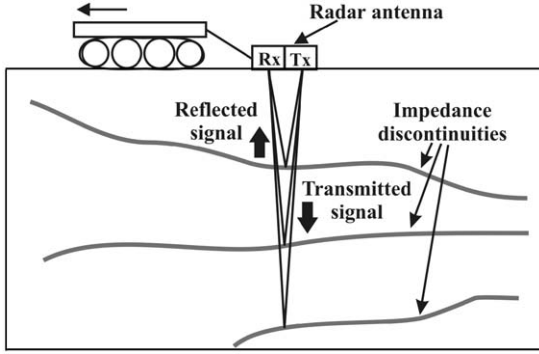


Fig. 4. The GPR working principle.

to map structure and features buried in the ground (Annan, 1992). In the basic GPR configuration, a transmitting antenna emits an e.m. impulse, which can be reflected or scattered by an intrinsic impedance discontinuity in the ground, and gathered by the receiving antenna (Fig. 4). The transmitted pulse length should be short enough (typically < 20 ns) to provide “resolvable” reflections (see further).

We recall that the e.m. properties of a material can be described by the following parameters:

(a) The relative complex permittivity, already mentioned in Section 2 (see Eq. (2)). In this case, however, the ϵ''_d term, which is the frequency-dependent loss related to the relaxation and polarization response phenomena, cannot generally be neglected in the GPR frequency range. The “low-frequency” loss effect related to conduction of free-charged particles is also taken into account through the DC conductivity σ .

(b) The relative complex magnetic permeability

$$\mu^* = \mu' - j\mu'' \quad (5)$$

where the imaginary part of permeability is related to magnetic losses.

The e.m. properties of geological materials can be dispersive and dissipative, and affect the propagation velocity and the attenuation of GPR pulses in the soil.

Considering the propagation of radio pulses in the ground, as a first approximation, we can refer to the velocity of a uniform wave in a homogeneous material, which is given by the relation $v = \omega/\beta$, where β is the wave phase constant corresponding to the real part of the medium complex wavenumber (or propagation constant) $k = \omega(\mu^*\epsilon^*)^{1/2}$:

$$\beta = \frac{\omega}{\sqrt{2}} \sqrt{\mu_0 \epsilon_0 \sqrt{\mu' \epsilon' - \mu''(\epsilon''_d + \sigma/\omega \epsilon_0) + |\mu^* x| \epsilon^*}} \quad (6)$$

In a low-loss medium, the speed of radio waves reduces to $v = c_0/(\mu' \epsilon')^{1/2}$ where c_0 is the velocity of light in a vacuum (in fact, in the low-loss case the phase constant β can be written as $\beta = k_0(\mu' \epsilon')^{1/2}$, where k_0 is the wavenumber in a vacuum).

Some materials, like ice, are virtually transparent to radio waves while others, like water-saturated clay, are practically opaque (they absorb or reflect the waves). Due to

the mismatch in the intrinsic impedance of the medium ($\eta = (\mu^*/\epsilon^*)^{1/2}$) between adjacent layers, reflections of the e.m. incident waves give rise, as described in the well-known equation for “normally incident” plane waves

$$R = (\eta_2 - \eta_1)/(\eta_2 + \eta_1), \quad (7)$$

where R is the reflection coefficient for normal incidence on a planar surface, and η_1 and η_2 are the intrinsic impedances in the first and second layer, respectively.

Various factors affect the radio wave signal propagating into a medium, e.g.:

(i) Energy loss in correspondence to each boundary between two layers, due to reflection/transmission process.

(ii) Scattering phenomena, when in the subsurface there are objects (inclusions) having the dimension typically of the same order of magnitude of the wavelength (e.g. Mie scattering for spherical particles). These inclusions scatter the e.m. energy in a random fashion, causing reduction of received power and clutter noise in the radar section.

(iii) Geometrical propagation spreading phenomenon of isotropic radiation (typically proportional to $1/r^2$ as in spherical waves).

(iv) Attenuation and dispersion caused by the e.m. properties of the medium in which the radio waves propagate. This parameter is affected by conductivity σ , complex permittivity ϵ^* , and complex permeability μ^* , and is a function of the frequency (dispersive phenomena).

For a material the attenuation constant α is given by the imaginary part of the complex wavenumber k and, for low-loss media, can be described by the equation

$$\alpha \cong \frac{k_0}{2} \left(\mu'' \sqrt{\frac{\epsilon'}{\mu'}} + \epsilon'' \sqrt{\frac{\mu'}{\epsilon'}} \right). \quad (8)$$

The main factors affecting radar signal range in the ground are radar system performance, attenuation in the ground and the reflection properties at boundary where the e.m. properties vary. The radar signal range can be determined from the expression (Annan, 1992)

$$Q = 10 \log \left(\frac{\xi_T \xi_R G_T G_R c^2 g \sigma_c e^{-4\alpha L}}{64\pi^3 f^2 L^4} \right), \quad (9)$$

where Q is the system performance or ratio of the transmitter signal amplitude to the minimum receiver sensitivity (expressed in dB), ξ_T the transmitter antenna efficiency, ξ_R the receiver antenna efficiency, G_T the transmitter antenna gain, G_R the receiver antenna gain, L the distance to the target, α the attenuation in the medium, f the frequency, g the backscattering gain of the target, and σ_c the target scattering cross-section area.

By considering the attenuation in geological materials and its frequency dependence, it follows that, for a given signal detection threshold, the maximum depth of investigation decreases rapidly with increasing frequency. In fact, many of the GPR systems are designed to operate at frequencies less than 1 GHz.

Table 1

Attenuations values and skin depth calculated for different Martian analogues at two different operation frequencies

Martian soil simulants	225 MHz		900 MHz	
	Attenuation (dB m ⁻¹)	Skin depth (m)	Attenuation (dB m ⁻¹)	Skin depth (m)
CO ₂ powder	0.02	357.1	0.10	89.4
CO ₂ powder+volcano sand	0.51	16.9	2.06	4.2
Dry volcano sand	0.65	13.3	2.61	3.3
Glass beads+magnetite (15 wt%) ^a	0.81	10.7	3.25	2.7
Magnetite grains (100%) ^a	5.51	1.6	22.06	0.4
Icy soil (20 wt% H ₂ O ice)	5.23	1.7	20.92	0.4
Basalt (dry)	0.21	40.6	0.86	10.2

^aGrain size range: 200–500 μm.

Another relevant aspect, which characterizes the GPR performance, is the vertical resolution, which expresses the ability of the system to distinguish between two subsequent signals close to each other in time. The shorter the time pulse width, the better is the resolution. Note however that, as the pulse width Δt decreases, the frequency bandwidth Δf increases introducing dispersion effects in the medium because the ground acts as a low-pass filter.

The upper limit of the resolution is related to the wavelength in the medium, being in fact limited to about a quarter of the wavelength of the incident radiation. Therefore, to obtain a detailed imaging of the subsurface the use of high-frequency antennas is required, although this will reduce the penetration depth of the GPR signal. The choice of the antenna frequency entails an accurate evaluation of the tradeoff between resolution and penetration depth, taking into account the main requirements imposed by the aim of the survey. Indeed, in the determination of the GPR performance, we have to consider that MUSES is envisioned for supporting the decision processes for the sampling-drilling activity of a system designed for a maximum depth of 1–2 m. Short prospecting depths and high resolutions have to be therefore preferred to deeper performance, that, however, would imply less accurate determination of the target details.

3.4. Attenuation, penetration depth and GPR 1-D modeling of Mars shallow subsurface

It is well known that GPR performance is maximized when it is applied in a very “resistive” environment, like that expected in a cold and dry planet. Very little is known on the e.m. properties (permittivity, permeability, and conductivity) of the Martian soil, but the absence of water on surface and in the shallow subsurface should in principle assure a good penetration of the signal. It is important to note, however, as already mentioned in Section 1, that measurements from the GRS experiment onboard the Mars Odyssey spacecraft (Boynton et al., 2002; Feldman et al., 2002; Mitrofanov et al., 2002) support the existence of significant quantities of

shallow subsurface water ice in certain parts of the planet. Furthermore, it has been pointed out (Olhoeft, 1998a, b; Heggy et al., 2001) that a high iron oxide content in the Martian subsurface, like the one found by both Viking and Pathfinder (Morris et al., 2001 and references therein), could strongly increase both dielectric and magnetic losses, significantly reducing the maximum penetration depth.

In order to evaluate the attenuation of the e.m. waves in the first few meters of the Martian soil, taking into account both the presence of the ice and the iron oxides, some calculations have been developed using Eq. (8) on the basis of permittivity and magnetic permeability data collected in laboratory (unpublished data). Table 1 summarizes the attenuation and the skin depth obtained in some Martian analogues at two different frequencies, whereas Table 2 shows the nominal resolution achievable in the same Martian analogues with the two operating frequencies.

The maximum depth of a detectable interface has been calculated using Eq. (9) with the following parameters: system performance $Q=134$ dB; transmitter antenna efficiency $\xi_T=-20$ dB; receiver antenna efficiency $\xi_R=-20$ dB; transmitter antenna gain $G_T=3$ dB; receiver antenna gain $G_R=3$ dB. In addition, different backscattering values g have been used depending on the soil model and frequency. A rough interface surface has been assumed for all cases. The maximum depth L (as a function of the attenuation α of the specific material, calculated with Eq. (8)) has been estimated for the two antenna frequencies (225 and 900 MHz) using the *PulseEkko* Software version 4.2 (Sensors and Software Inc., Mississauga, Ont., Canada). Table 3 shows the L values obtained for rough interfaces between different materials, where a two-layered soil model has been considered.

Furthermore, on the basis of the same soil parameters, synthetic radargrams have been calculated using a 1-D radar simulator. This simulator generates a synthetic radar trace by using a series of reflectivity coefficients (which represent the boundaries between different layers) and by convoluting these values with a wavelet that represents the impulse transmitted by the antenna. The specific simulator used in this work (*PulseEkko* Software) is based on the assump-

Table 2
GPR vertical resolution calculated at 225 and 900 MHz on the basis of laboratory data

Martian soil simulants	ϵ'	μ'	v (m/ns)	$\lambda/4$ (m)	
				225 MHz	900 MHz
CO ₂ powder	1.39	1.00	0.25	0.28	0.07
CO ₂ powder+volcano sand	2.05	1.00	0.21	0.23	0.06
Dry volcano sand	3.00	1.01	0.17	0.19	0.05
Glass beads+magnetite (15 wt%) ^a	4.54	1.32	0.12	0.14	0.03
Magnetite grains (100%) ^a	14.73	4.82	0.04	0.04	0.01
Icy soil (20 wt% H ₂ O ice)	5.00	1.00	0.13	0.15	0.04
Basalt	6.20	1.00	0.12	0.13	0.03

^aGrain size range: 200–500 μm .

Table 3
Maximum penetration depth calculated with radar range equation at two different frequencies

Material interfaces	L_{max} (m)	
	225 MHz	900 MHz
CO ₂ powder+volcano sand/volcano sand	13.6	3.4
Glass beads+magnetite (15 wt%)/icy soil	7.7	1.9
Magnetite grains (100%)/icy soil	3.6	0.9
Icy soil/basalt	2.7	0.7
Dry volcano sand/icy soil	12.5	3.1

tion that a plane wave is normally incident on a flat-layered soil model. The code transforms this model, consisting of user-defined layers of specified thickness, into an equivalent time-thickness-layered model. Then it computes all reflection and transmission coefficients using Fresnel equations, taking into account the ϵ' , μ' , and α values input for each layer. Multiples, interlayer reflections and spreading losses are included. Finally, the model produces the single traces, plotted 20 times to simulate a radar section.

The adopted soil models are presented in Fig. 5 for three possible planetary environments (models 1, 2, and 3); in particular, model 3 has been built based on Odyssey data. Figs. 6–8 show the synthetic radargrams calculated for each model, again at the frequencies of 225 and 900 MHz. Notice that the use of the two frequencies is crucial because it allows resolving thin layers at shallow depth (with 900 MHz antenna), as well as ensuring a high penetration in lossy materials (with 225 MHz antenna).

3.5. TDEM working principle

TDEM is a controlled source, remote sensing, time domain method, sensitive to the subsol conductivity gradient. The system consists of a transmitting antenna and one (or more) receiving antenna placed on the surface with respect to a chosen configuration (see Fig. 9).

The transmitting antenna (a loop, from hereafter TX) is fed by a square wave current which generates a sharp varia-

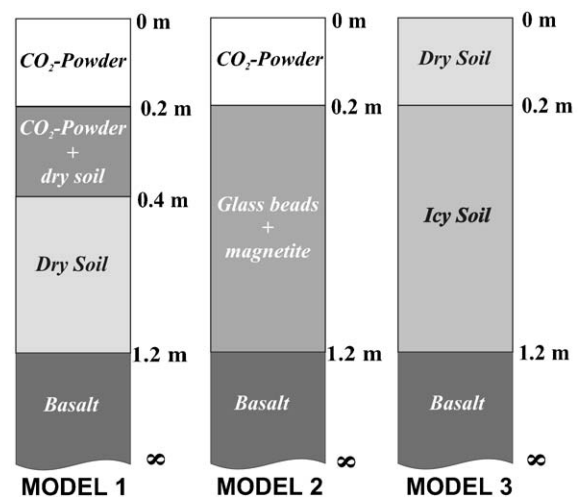


Fig. 5. Models of the Martian shallow soil adopted to calculate synthetic radargrams.

tion in time of the e.m. field (the primary field). The receiving antenna (a loop or a coil, from hereafter RX) is sensitive to the time rate of change of the vertical magnetic field. This is recorded at different time windows (from early to late time), each window containing the information about the medium conductivity at different depths (parametric sounding).

The propagation of the magnetic field through the soil is determined by a diffusion mechanism that is due to the effects of currents induced (according with the Faraday's law of induction) in the soil at various depths. These currents represent an image, in the soil, of the primary TX loop, which, once the primary magnetic excitation is ended, starts to decay with a time constant proportional to the local ground conductivity, generating a secondary field which propagates in any direction. While the primary field excites progressively deeper and deeper layers of soil, the secondary field, after a certain delay, is detected back by the RX loop. The amount of delay, the strength and the shape of the recorded signal characterize completely the geoelectrical structure of the medium (from few meters to kilometers).

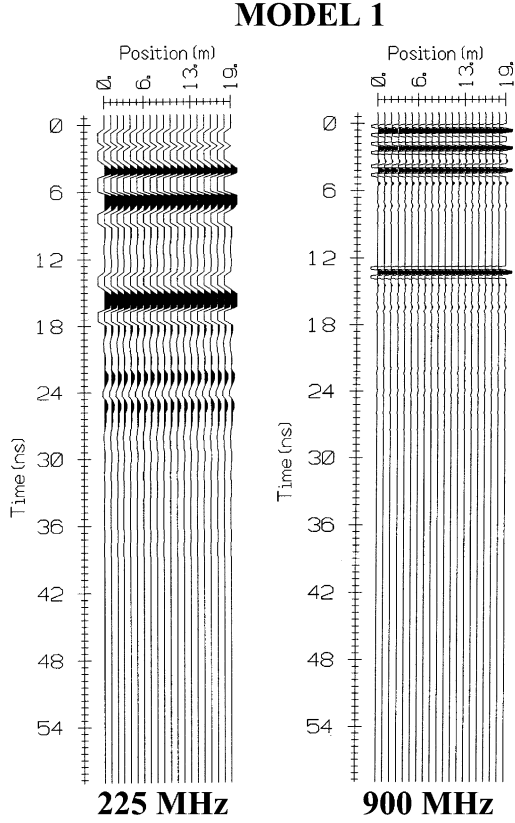


Fig. 6. Synthetic radargrams of MODEL 1 calculated for 225 and 900 MHz frequency. Notice that the first interface is detectable only with 900 MHz antenna.

The actual response of the system is in general a complex function of time, and soil conductivity and structure. The TDEM working principle is based on the diffusion inhomogeneous Helmholtz equations ($\tan \delta = \epsilon''/\epsilon' \gg 1$) (Ward and Hohmann, 1991)

$$\nabla \times \vec{e} + \mu \frac{\partial \vec{h}}{\partial t} = -\mu_0 \frac{\partial \vec{h}_{TX}^s}{\partial t} = -\vec{j}_m, \quad \nabla \times \vec{h} = \sigma \vec{e}. \quad (10)$$

The inhomogeneous term j_m is due to the magnetic TX loop perturbation. Eqs. (10) may be solved for the TDEM concentric configuration (see details in Filippini, 2002). The following assumptions hold:

(i) the TX antenna is a loop of area S_{TX} , placed above the ground surface at $(0, 0, h)$, $h < 0$ (by convention the z -axis is directed downward the surface), and is driven by a current $i(t)$;

(ii) the RX antenna is a multi-turns (n_{RX}) loop of area S_{RX} , sensitive to the vertical component of the magnetic field and placed at $(0, 0, h')$, $h' < 0$.

The measured signal at the receiver is

$$V(t) = -\frac{\partial}{\partial t} \left[\mu_0 n_{RX} \int_{S_{RX}} h_z(t, x, y, h', h) dS_{RX} \otimes i(t) \right], \quad (11)$$

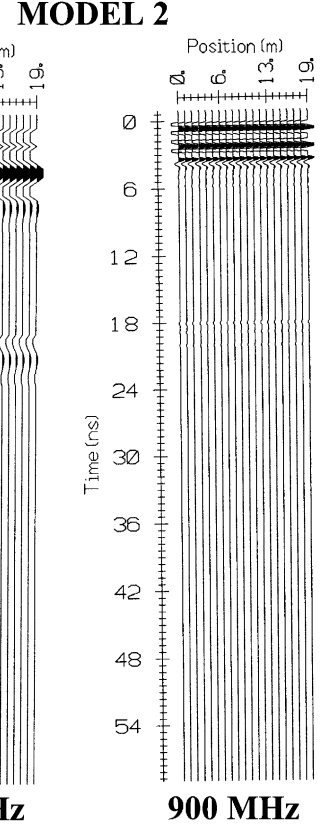


Fig. 7. Synthetic radargrams of MODEL 2 calculated for 225 and 900 MHz frequency. Notice that the first interface is detectable only with 900 MHz antenna. Moreover the interface between the glass beads + magnetite soil and basalt is visible only with the low-frequency antenna, due to the high attenuation of the magnetic material.

where h_z is the impulse response of the magnetic field vertical component and is related to the medium Green function (Filippini, 2002), which depends on the subsoil conductivity distribution.

The estimation of the subsoil conductivity is the result of the data inversion process, which is deeply discussed in Hohmann and Raiche (1991).

The above expression can be rearranged in order to describe the TDEM system as a communication channel between the TX and the RX, thus obtaining an input–output representation

$$\begin{aligned} \frac{V(\omega)}{I(\omega)} &= -i\omega\mu_0 n_{RX} \int_{S_{RX}} H_z(\omega, x, y, h', h) dS_{RX} \\ &= C(\omega). \end{aligned} \quad (12)$$

The solution of Eq. (12) is only numerically achievable with the exception of the homogeneous half-space. In these conditions, we obtain a simple expression of the transfer function of the system, which relates the TX current (I_{TX}), the area of the TX loop (S_{TX}), the subsoil conductivity (σ) and the received signal time delay (t), to the voltage induced

MODEL 3

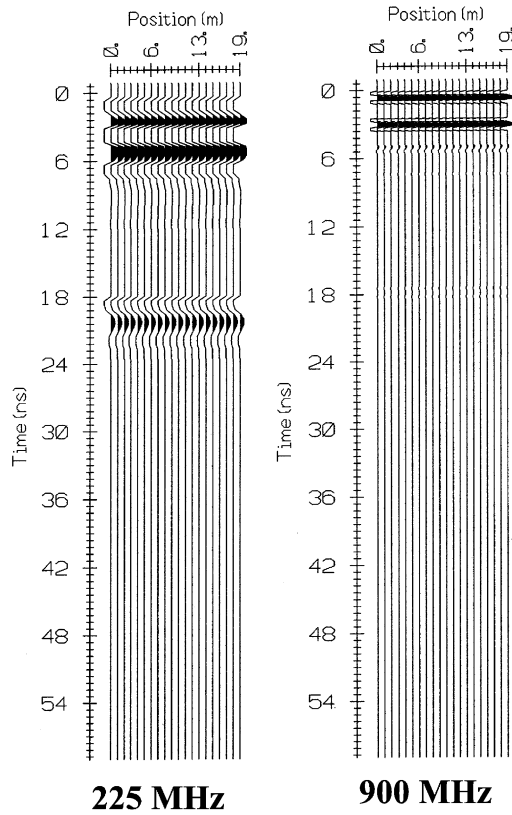


Fig. 8. Synthetic radargrams of MODEL 3 calculated for 225 and 900 MHz frequency. Notice that the first interface is detectable only with 900 MHz antenna. Again, the presence of a lossy material (icy soil) does not allow the detection of the deeper interface with the higher frequency antenna.

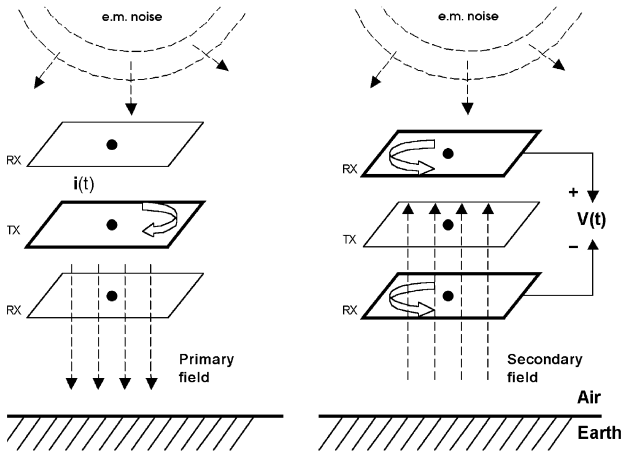


Fig. 9. TDEM working principle.

in the receiving loop RX:

$$V(t) = \frac{kM\sigma^{3/2}}{t^{5/2}}, \quad (13)$$

where $V(t)$ is the received voltage, $M = I_{TX} \cdot S_{TX}$ represents the primary magnetic dipole moment, and k is a constant

(Zhadanov and Keller, 1998; Nabighian and Macnae, 1991; Ward and Hohmann, 1991).

Eq. (13) shows the received voltage response vs. time, and even though it is not explicitly indicated, provides information on the subsoil conductivity at the different depths. This allows the identification of the discontinuities, whose depth can be estimated by considering that the diffusion speed of the field perturbation through the medium is

$$v_d = (2\mu_0\mu'\sigma t)^{-1/2}. \quad (14)$$

Once assumed a given conductivity, Eq. (14) can be used to estimate the time windows needed to sample the RX voltage in correspondence of a certain depth (the time sample is calculated by considering the two-way travel path of the perturbation, i.e. the time integral of (14)). If we assume, for example, a soil conductivity $\sigma = 0.01 \text{ S m}^{-1}$, Eq. (14) gives times of 0.63 and 63 μs , which correspond to depths of 5 and 50 m, respectively. Notice that lower conductivities require much shorter time windows.

By analyzing the time response, it is possible to detect the presence of targets (e.g. water) embedded in the subsoil. The simplest target for a TDEM sensor is conceived as a finite discontinuity within the vertical homogeneous conductivity profile. The presence of the discontinuity originates a time response (the perturbed response) which differs from the uniform model response (the reference model). A way to enhance any discontinuity within the medium geoelectrical structure is to treat the measured time response with the Fréchet's derivatives. Through the Fréchet's derivatives it is possible to define the sensitivity functions of the time response with respect to some soil model parameters (for instance, target conductivity) as (Zhadanov and Keller, 1998)

$$S_V(t) = \frac{V'(t) - V(t)}{V(t)} \frac{1}{\Delta\sigma}, \quad (15)$$

where $\Delta\sigma$ is the conductivity contrast between the target layer (having given conductivity σ_t , depth and thickness) and the background reference soil ($\Delta\sigma = \sigma_t - \sigma$).

In the numerical simulation (EMMA version 1.1, Hydro-Geophysics group, Aarhus University, Denmark) presented in Fig. 10, a target discontinuity, embedded in a homogeneous reference soil of conductivity $\sigma = 0.01 \text{ S m}^{-1}$, is considered. A 100 A m² energizing moment is assumed with identical TX and RX square loops of area 0.64 m² placed in concentric configuration. The discontinuity lies at 50 m below the surface, it is 10 m thick and assumes the values $\sigma_t = 0.1, 0.04$ and 0.02 S m^{-1} which correspond to $\Delta\sigma = 9\sigma, 3\sigma$ and σ , respectively. Notice that in such simulations the possible e.m. background noise has been neglected.

3.6. TDEM configuration for MUSES

For MUSES, the TDEM system is envisaged with the RX and TX loops arranged in the concentric null coupled configuration qualitatively shown in Fig. 9 (Nabighian and Macnae, 1991). This configuration is the less sensitive to

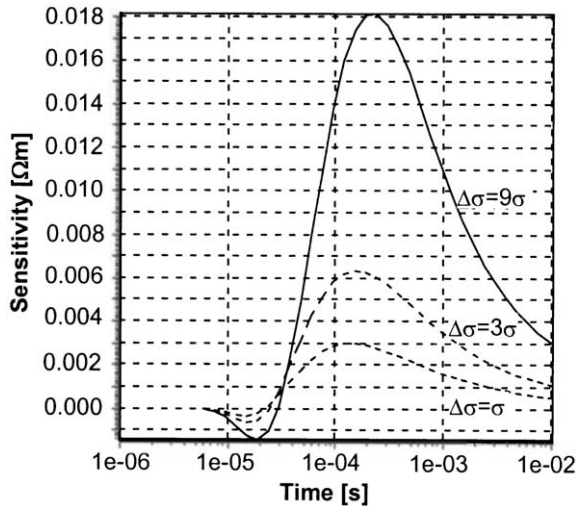


Fig. 10. Numerical simulation for a layer (10 m thickness) embedded at a depth of 50 m in a homogeneous half-space of conductivity $\sigma = 0.01 \text{ S m}^{-1}$, for three different values of conductivity perturbations ($\sigma_i = 0.1, 0.04$ and 0.02 S m^{-1}) (i.e. $\Delta\sigma = 9\sigma, 3\sigma$ and σ , respectively).

the lateral variations of the medium conductivity and, because of the reduced dimension, it is the most suitable to be housed onboard a rover or a mobile robot. Moreover, the null coupling between TX and RX (by subtracting the common signal) permits to enhance the reception at very early time.

The TX multi-turns antenna would permit to amplify the energizing moment, thus limiting the absorbed power. The number of turns and the receivers can be configured depending on the kind of experiment to be conducted (investigation modes). Two investigation modes have been assumed: shallow mode (single turn, low energized, two receivers, early time recording) and deep mode (multi-turns, high energized, single receiver, late time recording).

The system performance, in terms of voltage vs. penetration depth, is shown in Fig. 11, assuming a Gaussian noise with a white spectrum, and amplitude of 1 nV rms at the receiver input. The simulation has been performed assuming $\mu' = 1$ and two conductivity values ($\sigma_1 = 0.001 \text{ S m}^{-1}$ and $\sigma_2 = 0.0001 \text{ S m}^{-1}$). The results shown in Fig. 11 refer to the two operating modes, deep (time window 1–100 μs) and shallow (10 ns–1 μs). Shallow mode TX is almost a thousand times less energized than deep mode TX. The graphs have been obtained combining Eqs. (13) and (14), considering that the depth is related to the time through the diffusion velocity. For the given example, the expected range of investigation is about 3–300 m (the upper bound depends on soil conductivity), as at larger depth the signal is substantially masked by the noise.

Simulations carried out with higher magnetic permeability have shown an extension of the TDEM response to the later times and an increase of the received signal respect to the purely conductivity effect. Thus, magnetization effects should be taken into account for a correct TDEM

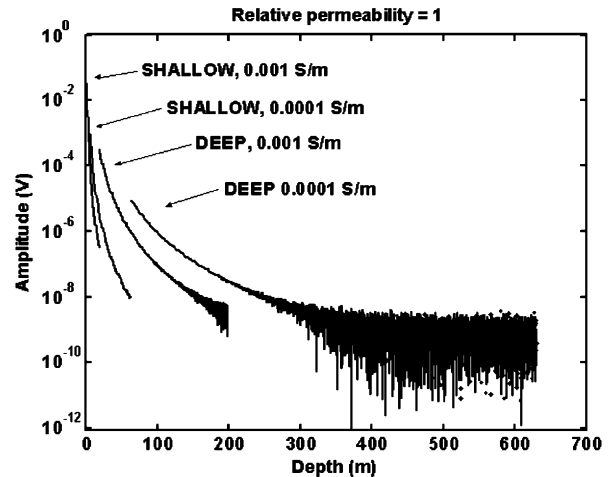


Fig. 11. TDEM performance, in terms of voltage vs. penetration depth, for a uniform half-space ($\sigma_1 = 0.001 \text{ S m}^{-1}$, and $\sigma_2 = 0.0001 \text{ S m}^{-1}$, $\mu_R = 1$) in presence of noise.

data interpretation. A further effect of iron oxide minerals is that magnetic relaxation losses can occur due to frequency dependent permeability. This phenomenon is known as magnetic viscosity or supermagnetism and has been observed in magnetite, hematite and maghemite (Olhoeft and Strangway, 1974; Grimm, 2002). This phenomenon, which could be of potential interest in Mars exploration, requires a specific analysis that, however, cannot be specifically treated within the limits of this paper.

4. Discussion on data fusion and conclusions

In a data fusion framework, different sensors are arranged in a multi-level hierarchical architecture (Hall and Llinas, 1997) wherein the information (raw or already processed data) interacts in:

- (i) competitive way (i.e. more sensors give information on the same object);
- (ii) cooperative way (i.e. some sensor observations rely on the results from other sensors);
- (iii) complementary way (i.e. sensors give partial non-overlapping, independent information).

To improve the target detection-estimation and classification-interpretation processes, MUSES, with reference to the sensor performance summarized in Table 4, implements the data fusion approach as follows. At *features level*, the *competitive* parameters extracted by SDSP and GPR (since they cover overlapped regions) are recursively processed to reduce uncertainty on the final feature vector. SDSP provides the measured dielectric constant and conductivity to GPR, which uses them to fine tune its data inversion process (i.e. to obtain the distance between subsoil interfaces). In turn the resulting GPR feature vector is fed-back to SDSP, which

Table 4
General specifications of MUSES sensors

	Quantities	Frequency (Hz)	Depth range (m)
SDSP	ε_i^*, H_i	100–10 ⁶	0–1
GPR	ε_i', H_i	$\cong 10^9$	0–10
TDEM	σ_i, H_i	Time domain	3–100

may refine its local estimation. Once the feature vector associated to the first meters (e.g. 10 m) is estimated, it is passed to the TDEM which uses it in a *cooperative* way to initialize its data inversion process (the zero step), i.e. setting the first layers to the values carried out by SDSP and GPR and estimating the feature vector for the deeper unknown layer.

Following a sequential fusion rule (Geraniotis and Chau, 1990) and by fusing the *complementary* information (in terms of depth range, measured parameters, operating conditions) collected by the three sensors, a vertical profile of the subsoil e.m. discontinuities is obtained. Complementary operation is also evident when the e.m. sounder works in unfavorable scenarios, i.e. very conductive or very resistive subsurface at shallow depths. In fact, while the TDEM is inadequate for investigation on highly resistive subsurface soils, since the transient vanishes at very early times and the results are not detectable by the receiver, the GPR fails when working in highly conductive scenarios, since the propagating wave is attenuated and does not penetrate in the subsoil. The presence of the two sensors prevents from failure in the case one of the above mentioned extreme working conditions occurs, since the blind sensor is complemented by the other.

In conclusion, MUSES fusion process results in a self-improving architecture, capable of reinforcing the overall final decision, since each sensor mutually enhances the other's performance by using the described cycle of local feature extraction, tuning and feed-back. SDSP and GPR cooperate in order to reduce uncertainties on shallow subsoil information (1–2 m), which are the most critical for exobiology research tasks and are of help for a decision process of sampling-drilling activities on a rover, while TDEM allows to extend the range of investigation to provide information on the deeper strata to improve the global geological knowledge.

Finally, it is important to consider that the e.m. soil parameters obtained from MUSES can be used as ground truth by other experiments that require the knowledge of the shallow subsoil permittivity to improve the data inversion accuracy of their observations (e.g. orbiting radar experiments).

Acknowledgements

This work has been partially supported by the Italian Space Agency (ASI) under the Contracts ACQUA and

TESEO, and by the European Space Agency (ESA) in the frame of the Topical Team on "Electromagnetic and Other Geophysical Techniques for In-Situ and Orbital Planetary Exploration". The authors would like to thank Sensors and Software for the use of the PulseEkko software. Furthermore the authors are sincerely grateful to Dr. Gary Olhoeft for the very helpful suggestions given in paper revision.

References

- Annan, A.P., 1992. Ground penetrating radar. Workshop Notes Sensors and Software, Ont., Canada (aannan@sensoft.ca).
- Boynton, W.V., Feldman, W.C., Squyres, S.W., Prettyman, T.H., Bruckner, J., Evans, L.G., Reedy, R.C., Starr, R., Arnold, J.R., Drake, D.M., Englert, A.J., Metzger, A.E., Mitrofanov, I., Trombka, J.L., D'Uston, C., Wanke, H., Gasnault, O., Hamara, D.K., Janes, D.M., Marcialis, R.L., Maurice, S., Mikheeva, I., Taylor, G.J., Tokar, R., Shinohara, C., 2002. Distribution of hydrogen in the near-surface of Mars: evidence for subsurface ice deposits global distribution of neutrons from Mars: results from Mars Odyssey. *Science* 297, 81–85.
- Chelidze, T.L., Gueguen, Y., 1999. Electrical spectroscopy of porous rocks: a review—I. Theoretical models. *Geophys. J. Int.* 137, 1–15.
- Fechant, C., Buis, J.P., Tabbagh, A., 1999. In situ measurement of medium-frequency apparent permittivity using an electrostatic quadrupole. Application to the determination of water content of wheat. *Meas. Sci. Technol.* 10, 174–181.
- Feldman, W.C., Boynton, W.V., Tokar, R.L., Prettyman, T.H., Gasnault, O., Squyres, S.W., Elphic, R.C., Lawrence, D.J., Lawson, S.L., Maurice, S., McKinney, G.W., Moore, K.R., Reedy, R.C., 2002. Global distribution of neutrons from Mars: results from Mars Odyssey. *Science* 297, 75–78.
- Filippini, R., 2002. Note on a TDEM experiment for space mission applications. ISSIA-CNR Report, 7/2002, November 2002 (cinthya.ottonello@aleph.it).
- Geraniotis, E., Chau, Y.A., 1990. Robust data fusion for multisensor detection systems. *IEEE Trans. Inf. Theory* 36, 1265–1279.
- Grant, F.S., West, G.F., 1965. Interpretation Theory in Applied Geophysics. McGraw-Hill, New York, pp. 407–409.
- Grard, R., 1990a. A quadrupolar array for measuring the complex permittivity of the ground: application to Earth prospection and planetary exploration. *Meas. Sci. Technol.* 1, 295–301.
- Grard, R., 1990b. A quadrupole system for measuring in situ the complex permittivity of materials: application to penetrators and landers for planetary exploration. *Meas. Sci. Technol.* 1, 801–806.
- Grard, R., Tabbagh, A., 1991. A mobile four-electrode array and its application to the electrical survey of planetary grounds at shallow depths. *J. Geophys. Res.* 96, 4117–4123.
- Grimm, R.E., 2002. Low frequency electromagnetic exploration for ground water on Mars. *J. Geophys. Res.* 107 (E2), 1–29.
- Hall, D.L., Llinas, J., 1997. An introduction to multisensor data fusion. *Proc. IEEE* 85, 6–23.
- Heggy, E., Paillou, P., Ruffie, G., Malezieux, J.M., Costard, F., Grandjean, G., 2001. On water detection in the Martian subsurface using sounding radar. *Icarus* 154, 244–257.
- Hohmann, G.W., Raiche, A.P., 1991. Inversion of controlled-source electromagnetic data. In: Nabighian, N. (Ed.), *Electromagnetic Methods in Applied Geophysics*. Society of Exploration Geophysics, Tulsa, Oklahoma, pp. 469–502.
- Mitrofanov, I., Anmov, D., Kozyrev, A., Litvak, M., Sanin, A., Tret'yakov, V., Krylov, A., Shvetsov, V., Boynton, W., Shinohara, C., Hamara, D., Saunders, R.S., 2002. Maps of subsurface hydrogen from high energy neutron detector, Mars Odyssey. *Science* 297, 78–81.
- Morris, R.V., Golden, D.C., Ming, D.W., Shelfer, T.D., Jorgensen, L.C., Bell, J.F., Graff III, T.G., Mertzman, S.A., 2001. Phyllosilicate-poor

- palagonitic dust from Mauna Kea Volcano (Hawaii): a mineralogical analogue for magnetic Martian dust? *J. Geophys. Res.* 106 (E3), 5057 (2000JE001328).
- Nabighian, N., Macnae, J.C., 1991. TEM prospecting methods. In: Nabighian, N. (Ed.), *Electromagnetic Methods in Applied Geophysics*. Society of Exploration Geophysics, Tulsa, Oklahoma, pp. 427–479.
- Olhoeft, G., 1998a. Ground penetrating radar on mars. In: *Proceedings of the Seventh International Conference on Ground Penetrating Radar*, Lawrence, Kansas, pp. 387–392.
- Olhoeft, G., 1998b. Electrical, magnetic and geometric properties that determine ground penetrating radar performance. In: *Proceedings of the Seventh International Conference on Ground Penetrating Radar*, Lawrence, Kansas, pp. 177–182.
- Olhoeft, G.R., Strangway, D.W., 1974. Magnetic relaxation and the electromagnetic response parameter. *Geophysics* 39, 302–311.
- Pettinelli, E., Vannaroni, G., Cereti, A., Paolucci, F., Della Monica, G., Storini, M., Bella, F., 2003. Frequency and time domain permittivity measurements on solid CO₂ and solid CO₂-soil mixtures as Martian soil simulants. *J. Geophys. Res.* 108 (E4), 8029. doi: [10.1029/2002JE001869](https://doi.org/10.1029/2002JE001869).
- Reynolds, J.M., 1998. *An Introduction to Applied and Environmental Geophysics*. Wiley, New York, pp. 796.
- Tabbakh, A., Hesse, A., Grard, R., 1993. Determination of electrical properties of the ground at shallow depth with an electrostatic quadrupole: field trials on archaeological sites. *Geophys. Prospect.* 41, 579–597.
- Vannaroni, G., Del Vento, D., 2003. Soil dielectric spectroscopy probe (SDSP) for the ExoMars rover mission. IFSI-CNR Internal Report, IFSI-2003-11 (giuliano.vannaroni@ifsi.rm.cnr.it).
- Von Hippel, A., 1988. The dielectric relaxation spectra of water, ice, and aqueous solutions, and their interpretation—3. Proton organization and proton transfer in ice. *IEEE Trans. Electr. Insul.* 23 (5), 825–840.
- Ward, S.H., Hohmann, G.W., 1991. Electromagnetic theory for geophysical exploration. In: Nabighian, N. (Ed.), *Electromagnetic Methods in Applied Geophysics*. Society of Exploration Geophysics, Tulsa, Oklahoma, pp. 121–223.
- Zhadanov, M.S., Keller, G.V., 1998. *The Geoelectrical Methods in Geophysical Exploration*. Elsevier, New York.